PHILOSOPHICAL TRANSACTIONS OF THE ROYAL SOCIETY A MATHEMATICAL, PHYSICAL & ENGINEERING SCIENCES

A Study of the Oxidation Mechanisms of Some Austenitic Stainless Steels in Carbon Dioxide at 1123K by means of Charged-Particle Nuclear Techniques. I

P. Skeldon, J. M. Calvert and D. G. Lees

Phil. Trans. R. Soc. Lond. A 1980 **296**, 545-555
doi: 10.1098/rsta.1980.0192

A STUDY OF THE OXIDATION MECHANISMS OF SOME AUSTENITIC STAINLESS STEELS IN CARBON DIOXIDE AT 1123K BY MEANS OF CHARGED-PARTICLE NUCLEAR TECHNIQUES. I

BY P. SKELDON†, J. M. CALVERT‡ AND D. G. LEES†
† *Metallurgy Department, Manchester University, Manchester, M13 9PL, U.K.*
‡ *Physics Department, Manchester University, Manchester, M13 9PL, U.K.*

(*Communicated by R. B. Nicholson F.R.S. – Received* 10 *January* 1979)

[Plates 1 and 2]

CONTENTS

	PAGE
1. INTRODUCTION	546
2. PREVIOUS WORK	546
3. EXPERIMENTAL PROCEDURE	547
(*a*) Sample preparation	547
(*b*) Oxidation of samples	548
(*c*) Determination of ^{18}O concentration profiles	548
(*d*) Elastic scattering of charged particles	549
(*e*) Determination of the effective concentration of ^{18}O ions at the surface of oxide scales	550
4. RESULTS	552
(*a*) Oxide thickness	552
(*b*) Appearance of oxidized samples	552
(*c*) Composition of scales	552
(*d*) Scale morphology	552
(*e*) The ^{18}O tracer distributions	553
5. DISCUSSION	554
6. CONCLUSIONS	555
REFERENCES	555

The oxidation behaviour of a 20% (by mass) Cr, 25% (by mass) Ni, niobium-stabilized steel in carbon dioxide at 1123 K and a pressure of approximately 0.1 MPa has been investigated by using charged-particle nuclear techniques and conventional methods. The nuclear techniques were used to study the growth mechanism, thickness and surface composition of the oxide. The scale consisted of an outer spinel layer, a layer of Cr_2O_3 inside this and then a silicon-rich layer at the oxide–metal interface. The scale grew primarily by cation transport but some oxygen diffusion also occurred.

Vol. 296. A 1424. 43 [Published 18 April 1980

1. Introduction

The reaction between 20% (by mass) Cr, 25% (by mass) Ni, Nb-stabilized steel and carbon dioxide in the temperature range 923–1173 K has received much attention because this material has been selected for the fuel-cans in Advanced Gas-cooled Reactors. Yet despite the number of studies of the oxidation behaviour of this alloy, the processes involved have not been clearly elucidated. That is so is probably a result of the alloy composition, which gives rise to the formation of a thin scale composed of a number of different oxides.

In the present work we have used nuclear techniques developed at Manchester to investigate in detail the oxidation mechanisms of the 20% (by mass) Cr, 25% (by mass) Ni, Nb-stabilized alloy (which we will henceforth refer to as 'the standard steel'). In addition we have studied (*a*) the same alloy with a cerium treatment and (*b*) effectively the same alloy containing a dispersion of titanium nitride. The interest in the latter two alloys arises from recent attempts made to improve the standard steel; deposition of ceria (CeO_2) on the surface improves the oxide–metal adhesion and the TiN dispersion improves the creep strength. Our investigations of these alloys are the subject of separate papers (Skeldon *et al.* 1980*a*, *b*, subsequently referred to as II and III).

Table 1. Alloy composition (% by mass)

Fe	Cr	Ni	Mn	Si	Nb	C
bal.	20.6	25.6	0.5	0.57	0.46	0.02*

* Nominal value

2. Previous work

The composition of the standard steel is given in table 1. Francis *et al.* (1971) found that at 1123 K the oxidation rate in CO_2 at 0.027 MPa decreased continuously with time until, after 40–60 h, a slow linear rate was observed. The linear rate-constant varied from 0.9 to 1.9 μg/cm²/h. Antill *et al.* (1964) state that in long exposures there were no consistent or marked effects exerted by small amounts of carbon monoxide (5%), water vapour (1000 parts/10^6 by volume) or the total pressure (0.1–2.03 MPa) of the gas. The major part of the mass-gain when the alloy reacts with CO_2 is caused by oxide formation. Antill & Warburton (1967) observed a small pick-up of carbon during the initial stages of the reaction in pure CO_2 and then, for up to at least 700 h exposure at 1123 K, a slow, steady, decarburization. No experiments have been reported on the incorporation of carbon in the oxide-layer as it grows. The alloy forms a relatively complex scale consisting of Cr_2O_3 and a spinel which contains manganese, iron and chromium (Francis & Whitlow 1965). A thin layer, which is possibly amorphous silica, is present at the base of the scale. This layer is probably of the order of 10 nm thick, and the thickness does not appear to change with increasing oxidation time (Francis 1966). The distribution of the Cr_2O_3 and spinel in the scale is not certain. Francis & Whitlow (1965) suggested that it is at the oxide–gas interface, while on the basis of later work, Francis *et al.* (1968) suggested that it may be beneath the Cr_2O_3 layer.

When a gold marker was deposited on the surface of a sample and the sample was oxidized, the marker soon disappeared as the scale grew over it (Tyzack *et al.* 1974). This indicates that a significant proportion of the scale forms at the gas–oxide interface. This evidence is supported

by the observation of growth-steps on the oxide crystals at the scale surface (Fern & Antill 1970). Photographic observations of the oxidation by Fern & Antill showed that when the alloy was isothermally oxidized and then cooled, part of the scale spalled, revealing a surface of bright metallic appearance. However, on re-oxidation approximately 75% of the spalled areas were highly protective. Therefore the authors proposed that at the base of the scale there is a thin layer, probably of the order of 100 nm thick, which plays a major role in the protection of the steel. In view of the fact that small amounts of silicon are known to improve the oxidation resistance of stainless steel, and silicon has been found to concentrate at the oxide–metal interface on this alloy, they suggested that silicon is an essential constituent of this layer. However, Francis (1966) has shown that although the initial oxidation rate of a silicon-free steel was considerably higher than that of the basic steel, the subsequent oxidation rate (from 0.1 to 100 h) was lower. This is not what would be expected if diffusion through a silicon-containing layer were rate-controlling, although it is not conclusive because the oxides on the two alloys were not identical. During the photographic study of the oxidation by Fern & Antill (1970) transient increases in the rate were occasionally seen. These higher oxidation rates sometimes occurred locally and sometimes over the whole field of view. The area of the field of view was not stated, but from the dimensions and magnifications of photographs in the paper this may have been *ca.* 2×10^{-3} cm^2. The sudden rate increases were observed on average 1–3 times during the first 100 h of oxidation. It was proposed that the linear part of the oxidation kinetics may be explained by the scale continually cracking and rehealing at local sites, so that the individual accelerations in the oxidation rates were not observed, but combined to produce on average a constant oxidation rate. Hales *et al.* (1974) have proposed that diffusion of chromium in the alloy is the rate-controlling step in the growth of Cr_2O_3 on austenitic steels. They base this suggestion on data on the oxidation rates of steels, which show that in general oxidation of ferritic steels proceeds about an order of magnitude faster than that of austenitic material. They link this difference in oxidation rate with the fact that chromium diffusion in ferritic steels is faster than in austenitics. However, Evans *et al.* (1976) in a reassessment of the data show that there is no significant difference in the oxidation rates for the two types of steel.

In view of the very limited evidence on the growth-mechanism of the oxide on this alloy, and the need for more information on the distribution of elements within the oxide, the nuclear techniques described below have been used to study the oxidation behaviour in carbon dioxide at approximately 0.1 MPa and 1123 K.

3. Experimental procedure

(*a*) *Sample preparation*

Tubular samples of the alloy were supplied by Berkeley Nuclear Laboratories. The composition is given in table 1. The tube dimensions were 15.9 mm outside diameter and 0.7 mm wall thickness. The tube was cut into *ca.* 5 mm lengths and sectioned into quarters, which were then cleaned in soap solution, degreased in acetone and annealed for 1 h in a vacuum ($< 10^{-5}$ Torr) at 1233 K. This treatment left a thin interference film on the alloy surface. The samples were lightly polished down to 1 μm diamond powder and the dimensions measured. The samples were again cleaned in soap solution, degreased in acetone and finally weighed.

PHILOSOPHICAL TRANSACTIONS OF THE ROYAL SOCIETY A MATHEMATICAL, PHYSICAL & ENGINEERING SCIENCES

(*b*) *Oxidation of samples*

Oxidation times are given in table 2. Specimens were oxidised at 1123 K in static carbon dioxide, at approximately 0.1 MPa pressure. The samples were sequentially oxidized, first in natural carbon dioxide and secondly in carbon dioxide isotopically enriched in ^{18}O. The specimens were held at temperature when the gases were changed, and, at the end of the experiment, were cooled to room temperature *in vacuo*. For the sake of brevity, the natural carbon dioxide will sometimes be referred to as $C^{16}O_2$ and the isotopically enriched carbon dioxide as $C^{18}O_2$. The natural carbon dioxide was passed through anhydrous calcium chloride and over an activated catalyst to remove moisture and oxygen respectively.

TABLE 2. OXIDATION TIMES (IN HOURS)

no.	total	natural CO_2	$C^{18}O_2$
1	115.85	48.75	67.1
2	335.25	211.0	124.25

The isotopically enriched carbon dioxide, which initially contained 96 % $C^{18}O_2$, was stored at room temperature and 0.1 MPa pressure in a brass cylinder. This gas was transferred from the cylinder to the oxidation apparatus by freezing the carbon dioxide on a small-volume copper cold-finger immersed in liquid nitrogen. The carbon dioxide rapidly solidified and thus separated from any oxygen, nitrogen or carbon monoxide present. The maximum possible contamination of the carbon dioxide after separation was about 1 % (by volume).

The isotopically enriched gas is expensive and was therefore retrieved after each oxidation. The carbon monoxide produced by the oxidation reaction was collected and stored on a molecular sieve. Periodically, the carbon monoxide was converted to carbon dioxide by heating in the presence of CuO at 873 K. The regenerated carbon dioxide was added to the main store; thus the isotopic composition of the carbon dioxide was not the same for all oxidations. As a result of the changing isotopic composition of the gas, the term '100 % effective concentration of ^{18}O ions' will be used to refer to the concentration of ^{18}O ions found in the scale formed on a sample of alloy oxidized in the isotopically enriched gas alone, so that the percentage of ^{18}O nuclei in the scale is equal to that in the oxidizing gas. We call such a sample a reference specimen.

(*c*) *Determination of the* ^{18}O *concentration profiles*

The nuclear technique used in this investigation to determine the ^{18}O concentration profile has been discussed in detail elsewhere (Calvert *et al.* 1974) and therefore will only be described briefly here.

When ^{18}O nuclei are bombarded with protons, α-particles are produced by the reaction: $^{18}O + p \rightarrow {}^{15}N + \alpha$. The yield of particles from the reaction depends on the ^{18}O concentration and on the proton energy, and at certain energies there are sharp peaks (reasonances) in the yield.

High-speed charged particles moving through a solid lose energy at a rate determined by the speed and type of particle and by the density and chemical composition of the solid. The processes involved are reasonably well understood and the mean energy of a beam of particles of initial energy E_i, after penetrating to a given depth in a solid, can be calculated with confidence.

There is a strong resonance in the $^{18}O(p,\alpha)^{15}N$ reaction at an incident proton energy of 1.763 MeV; figure 1 is an aid to understanding how this resonance is used. For $E_i > 1.763$ MeV, the depth, x, at which the energy has been reduced to 1.763 MeV in a particular solid, can be calculated. The yield of α-particles from the resonance can be measured with a solid-state detector, and the yield is proportional to the ^{18}O concentration at the depth x. By making measurements at different energies E_i, the ^{18}O concentration can be determined as a function of depth x below the surface.

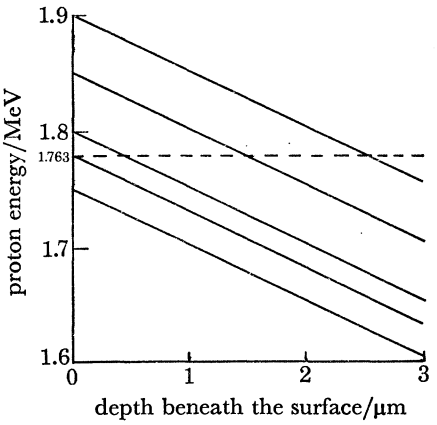

FIGURE 1. Graph showing the variation of proton energy with depth. (The dashed line corresponds to a proton energy of 1.763 MeV). The rate of energy loss depends upon the material; this figure has been drawn for TiO_2.

The above account is over-simplified because it ignores a number of factors that affect the measurement; the resonance occurs over a range of proton energies around 1.763 MeV; the primary beam has a finite energy-spread about the well-defined mean; the processes which determine energy-loss are statistical in nature and therefore this energy-spread increases as the protons travel through the solid; the detector has a finite energy resolution. The effect of these 'spreading factors' is that the graph of α-yield against incident proton energy does not correspond directly to a plot of ^{18}O concentration against depth, but is spread out or blurred with respect to it. To deal with this situation, computer programs have been developed by members of the team at Manchester (Neild *et al.* 1972) so that an ^{18}O concentration distribution can be assumed and allowance made for the various spreading factors by mathematical convolution to give a predicted graph of α-yield against incident proton energy, which is compared with the experimentally determined one.

(*d*) *Elastic scattering of charged particles*

When charged particles strike a solid they are elastically scattered with an energy which depends, among other things, on the atomic mass of the target nucleus. Therefore, analysis of the energy of the elastically scattered particles can be used to obtain the surface composition of a specimen. The thickness of a layer of oxide on the surface of an alloy can also be determined because the energy of these particles also depends upon the depth to which they penetrate the target before they are scattered. Thus particles scattered by oxygen nuclei at the oxide–metal interface have less energy than particles scattered from oxygen nuclei at the oxide–gas interface and the energy difference depends upon the oxide thickness. Also, particles scattered by metal

nuclei in the alloy have less energy than those scattered by metal nuclei in the oxide, and therefore the sharp change in metal concentration at the oxide–metal interface shows up on the spectrum of scattered particles.

The actual shape of the spectrum of elastically scattered particles is complex but the relevant features can be illustrated by consideration of the simple case of a Cr_2O_3 layer containing nickel on an effectively semi-infinite Cr–Ni alloy (see figure 2). There will be several contributions to the elastic spectrum. At the highest energy region there will be a yield of particles scattered from nickel nuclei in the Cr_2O_3 layer (curve A). At its lower energy end, (corresponding to particles passing through this layer and out again) curve A joins curve B, which corresponds to particles scattered from nickel nuclei in the alloy. Curves C and D correspond to particles scattered from chromium nuclei in the oxide and alloy respectively. Curve E arises from particles scattered from oxygen nuclei in the oxide. The actual spectrum is a summation of all these contributions. 4 MeV α-particles were used for surface analysis of the oxides; the oxide thicknesses were determined from the spectrum of elastically scattered protons which was obtained when the ^{18}O distributions were determined. Examples of actual spectra are given in II.

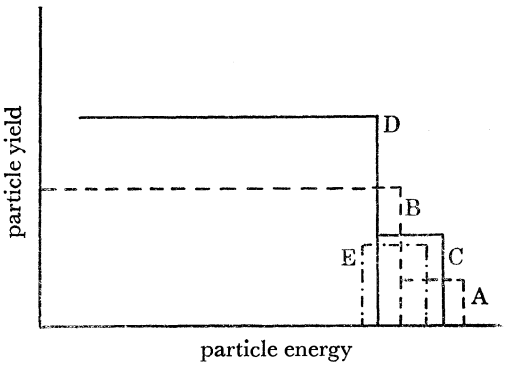

FIGURE 2. A schematic diagram showing the contributions to the spectrum of elastically scattered particles from a thin layer of Cr_2O_3 containing nickel, on a chromium-nickel alloy. Curve A arises from scattering from nickel nuclei in the Cr_2O_3 layer, curve B from scattering from nickel nuclei in the alloy, curves C and D from scattering from chromium nuclei in the oxide and alloy respectively, and curve E from oxygen nuclei in the oxide. The width of A (and of C and E) depends on the oxide thickness.

(*e*) *Determination of the effective concentration of* ^{18}O *ions at the surface of oxide scales*

A knowledge of the concentration of ^{18}O ions at the oxide-gas interface of a scale which was formed by oxidizing first in $C^{16}O_2$ and secondly in $C^{18}O_2$ is necessary to deduce the oxide growth-mechanism. This concentration was determined in the present investigation by comparing the α-yield from the surface of the specimen in question with that from a reference specimen when both specimens were bombarded with protons in identical experimental circumstances. The energy of the proton beam was selected so that the protons reached the resonance energy just beneath the scale surface; the large cross-section of the nuclear reaction at this energy gave a high yield of α-particles. The α-yields were normalized to an identifiable part of the spectrum of elastically scattered protons to ensure that the α-yields were compared for the same total proton charge. The feature of the elastic scattering spectrum that was chosen for the normalization in the present work was the step corresponding to elastic scattering from metal ions in the sample surface because this was generally easily distinguished. The ratio

of the normalized α-yields of the test and reference specimens expressed as a percentage gives the effective percentage concentration of ^{18}O ions in the surface of the test specimen.

There are various factors which must be considered when determining the effective concentration of ^{18}O ions in the surface of an oxide scale. For example, for some oxides, spalling tends to occur in a manner that produces many small areas of exposed alloy, giving the sample a speckled appearance. The proton beam, of approximately 1 mm diameter, is in these circumstances incident simultaneously on areas of oxide and of exposed alloy. The density of metallic ions in the surface after spalling is greater than that in the oxide alone, and this affects the yield from elastic scattering. In order to correct for this, the amount of spalled area is calculated by comparing the spectrum of elastically scattered protons from the test sample with that from a sample known to have a complete scale at the area of nuclear analysis. In the case of the alloys studied in this investigation there is a second factor to be considered because of the relatively complex composition of the scales. X-ray diffraction measurements showed that the scales consisted of a mixture of Cr_2O_3, possibly containing some Fe_2O_3 in solution, and spinel. These measurements apply to a greater area and a greater depth of the sample than do the associated Van de Graaff measurements. Because of the relatively small diameter of the proton beam, the areas being analysed in the test and reference samples respectively could well have differing relative amounts of the two metal oxides. This difficulty is resolved as follows. In comparing a specimen under test with a reference specimen, we wish to determine their relative ^{18}O concentrations allowing for any difference between the specimens of (i) oxygen concentration, and (ii) the type and concentration of metal ion, since normalization is based on the yield of scattered particles from the metal ions in the surface. If n_o is the density of oxygen ions in the specimen and n_m is the corresponding density of metal ions, f_i is the fraction of metal i and the suffices T and R indicate the test and reference specimens respectively, then the relative yields, Y, of α-particles from the $^{18}O(p,\alpha)^{15}N$ reaction are:

$$\frac{Y_T}{Y_R} = \frac{(n_o)_T\,(n_m)_R \sum_i f_{iR} Z_i^2}{(n_o)_R\,(n_m)_T \sum_i f_{iT} Z_i^2},$$

where Z is the atomic number. This expression assumes that the oxides in both specimens are grown in oxygen with the same enrichment of ^{18}O. The density of oxygen ions in Cr_2O_3 is *ca.* 1.16 times that in spinel, but the Z-dependent expression in the present case is less than 1 for these same oxides (since $Z_{Fe} > Z_{Cr}$) and so any uncertainty in the normalized yield because of differences of composition in the comparison with the test sample is less than the factor 1.16.

A third factor to be considered arises because of the width of the resonance in the nuclear reaction $^{18}O(p,\alpha)^{15}N$. If a comparison of normalized α-yields is made between scale in which the concentration of ^{18}O ions as a function of depth is constant, and one in which the concentration falls from the surface value, the surface concentration of ^{18}O will be underestimated in the latter case because the average concentration across the region of the scale in which protons are at the resonance energy will be lower than the surface value. The magnitude of the effect that this will cause in this case will depend upon the form of the concentration profile; it may be large if the concentration falls rapidly within 0.5 μm of the oxide surface. The relevance of this to the present work will be discussed in papers II and III.

4. Results

(*a*) *Oxide thickness*

The oxide thickness was calculated from elastic scattering, rather than mass gain measurements, because the latter could be affected by oxide spalling. The thickness of the oxide on sample 1 was 1.5 μm. The thickness of that on sample 2 was not measured because all the oxide spalled.

(*b*) *Appearance of oxidized samples*

Sample 1 formed an adherent scale with no signs of spalling; the major part was coloured grey-green although there were patches of alloy that appeared relatively unattacked, being of a dull metallic colour. Sample 2 formed a completely non-adherent scale which spalled in flakes of area approximately 1 mm^2 and was greyish-green in colour. The alloy surface had a dull metallic colour. (The specimen numbers refer to table 2.)

Table 3. X-ray diffraction results

oxide	Cr_2O_3	spinel
sample 1	medium	strong

Table 4. Energy dispensive X-ray analysis results

	Si	Cr	Mn	Fe	Ni
Flake of scale from sample 2	n.d.	87.2	11.0	1.8	n.d.†

† n.d. denotes not detected.

(*c*) *Composition of scales*

The results of X-ray diffraction measurements on sample 1 are given in table 3 and show that the scale consisted of a mixture of 'Cr_2O_3' and spinel; the diffraction peaks from the spinel were the stronger. (It should be noted that the presence of a small amount of Fe_2O_3 in the Cr_2O_3 would not be detected.) A flake of oxide from sample 2 was examined by energy-dispersive X-ray analysis. The results, which are given in table 4, show that the scale was chromium-rich with a significant amount of manganese. Very little iron and no nickel or silicon were detected. Elastic scattering experiments (with 4 MeV α-particles) identified chromium and either manganese or iron in the surface of the scale formed on specimen 1. (It was difficult to separate the edges corresponding to iron and manganese in the energy spectrum). Similar experiments on sample 2, from which the scale had spalled, indicated an enrichment of silicon at the alloy surface.

From these results we believe that the scale has a thin silicon-rich layer at the oxide–metal interface, next to this a Cr_2O_3 layer and then a manganese–iron–chromium spinel outer layer. This composition is the same as that proposed by Francis & Whitlow (1965) and does not support the suggestion made by Francis *et al.* (1968) that the spinel is underneath the Cr_2O_3.

(*d*) *Scale morphology* (figures 3–5, plates 1 and 2)

The main features shown by these pictures may be summarized as follows:

(i) the scale was not buckled, and oxide crystals projected from the surface;

(ii) the underside of the scale was sometimes covered with whiskers;

FIGURE 3. The surface of the scale on sample 1. Electron accelerating energy = 30 keV.

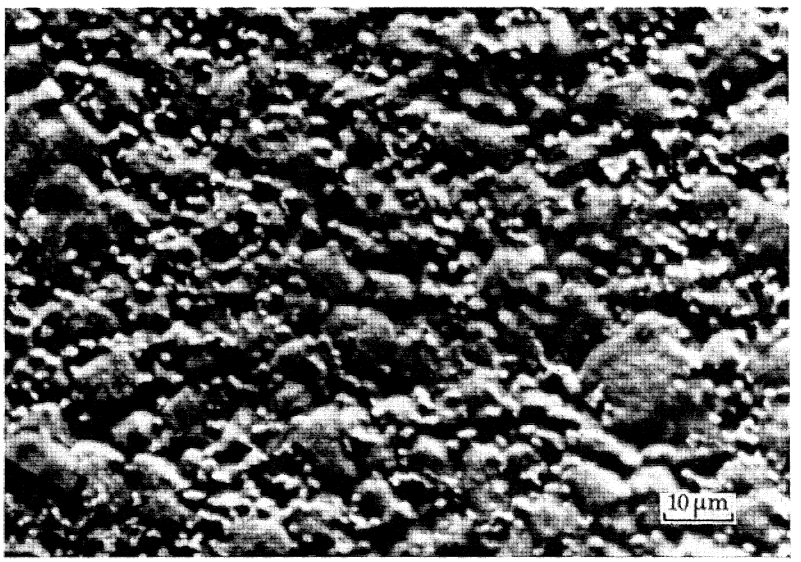

FIGURE 5. The surface of sample 2, after oxidation and spallation of the scale. Electron acceleration energy = 30 keV.

(*Facing p.* 552)

PHILOSOPHICAL TRANSACTIONS OF THE ROYAL SOCIETY A MATHEMATICAL, PHYSICAL & ENGINEERING SCIENCES

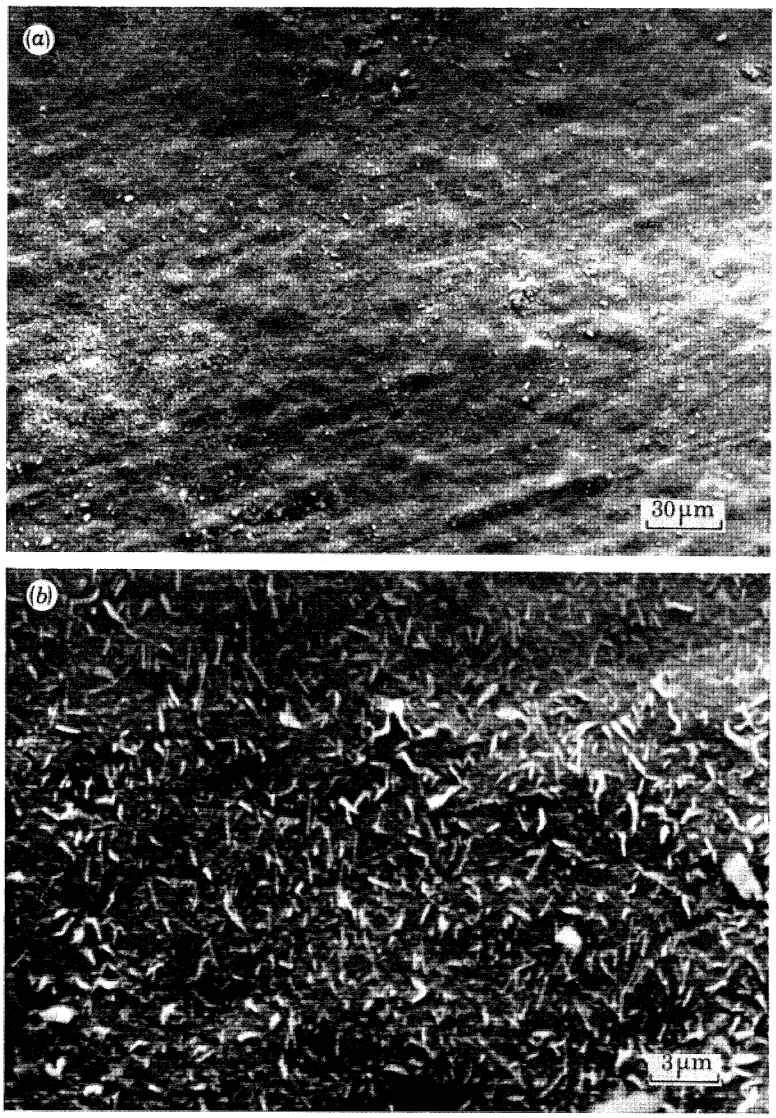

FIGURE 4. The underside of the scale formed on sample 2. Electron acceleration energy = 30 keV.

PHILOSOPHICAL TRANSACTIONS OF THE ROYAL SOCIETY A MATHEMATICAL, PHYSICAL & ENGINEERING SCIENCES

(iii) the grain size of the oxide at the gas interface appears to be much larger than that at the metal interface – the evidence presented in §4*c* suggests that he former is spinel and the latter is Cr_2O_3;

(iv) the surface of the alloy where the scale had spalled was rough.

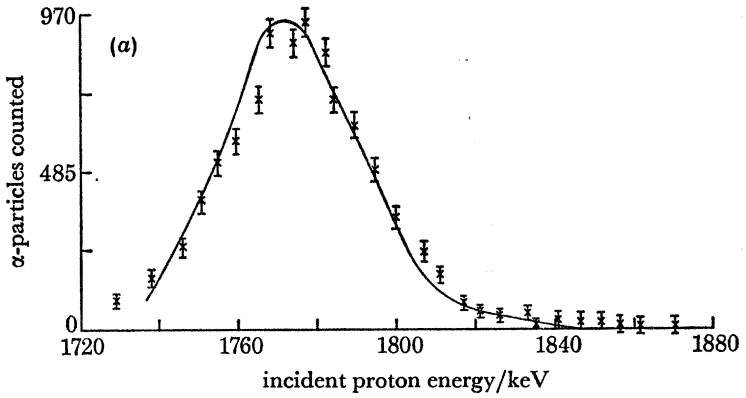

FIGURE 6*a*. A plot of α-particle yield against incident proton energy for the standard steel, sample 1. The continuous curve was computed for a step 0.65 μm thick.

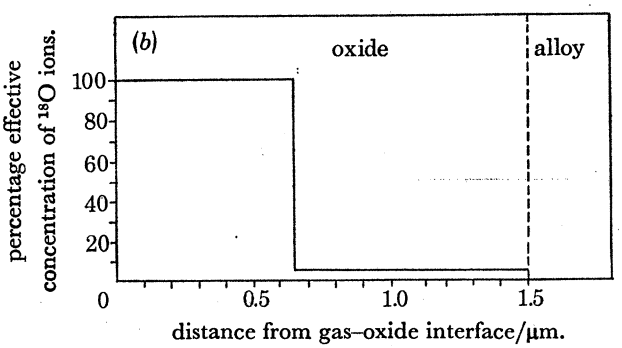

FIGURE 6*b*. The ^{18}O distribution deduced from figure 6*a*. It was difficult to determine accurately the shape of the concentration profile in the low-concentration region, and although it has been drawn as constant, it may decrease as the oxide–metal interace is approached.

(*e*) *The* ^{18}O *tracer distributions*

Figures 6 and 7 show the graphs of α-yield against incident proton energy for specimens oxidized first in CO_2 containing natural oxygen and then in $C^{18}O_2$, together with the ^{18}O concentration profiles which have been deduced from these graphs. For specimen 2 (figures 7*a*, *b*) the surface of the alloy from which the flake had spalled was examined by using 750 keV protons. (This is better for measuring the ^{18}O concentration of oxide layers $\lesssim 0.5$ μm.) A low concentration of ^{18}O was found at this interface, which is consistent with the presence of a thin layer of oxide, but there was no thick (>0.5 μm) layer of ^{18}O. (If a thin layer of oxide were present, it could be the silica layer proposed by Francis (1966).)

The principal features of the concentration profiles are:

(i) the bulk of the ^{18}O is located in a layer at the oxide-gas interface;

(ii) the effective concentration of ^{18}O in that layer is 100 %, within the limits of experimental error;

(iii) a low concentration (*ca.* 5%) of ^{18}O extends from the inside of the ^{18}O layer to the alloy–oxide interface;

(iv) there is no build-up of ^{18}O at the alloy–oxide interface;

(v) the ^{18}O layer has the form of a step, within the limits of experimental error, apart from the low concentration of ^{18}O which extends as far as the alloy–oxide interface.

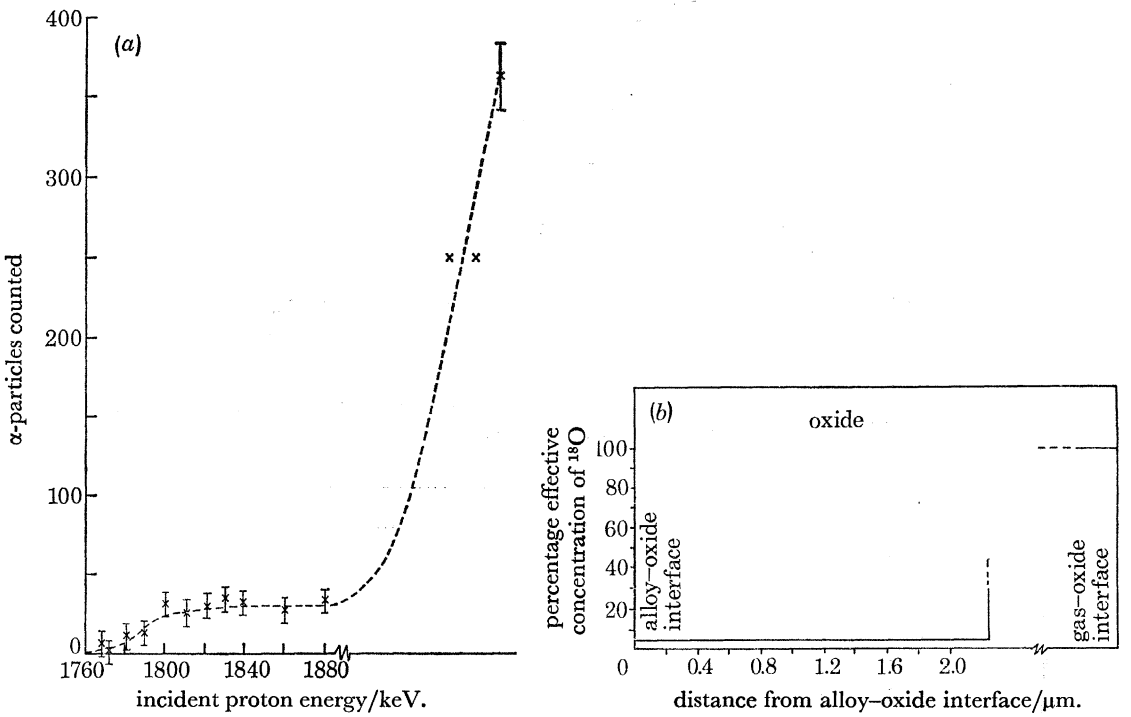

FIGURE 7*a*. A plot of α-particle yield against incident proton energy for a flake of oxide from the standard steel, sample 2. Most of the points were obtained with the proton beam incident on the oxide–alloy interface. The scale was too thick for a complete analysis, and so the beam was directed onto the oxide–gas interface and this showed that the effective concentration of ^{18}O at the surface of the scale was 100%.

FIGURE 7*b*. The ^{18}O distribution deduced from figure 7*a*. Note that there is no build-up of ^{18}O at the oxide–metal interface.

5. DISCUSSION

The evidence suggests that the scales consisted of an outer spinel layer, inside which was a layer of Cr_2O_3 and a silicon-rich layer at the oxide–metal interface. The ^{18}O tracer results showed that the scale grew primarily by cation diffusion and that a small amount of oxygen diffusion occurred. This is consistent with the fact that crystals projected from the outer surface of the oxide and that whiskers were present on the underside, and also with the observation of Tyzack *et al.* (1974) that a gold stripe was buried during the early stages of oxidation of this alloy. We are not able to determine the exact shape of the ^{18}O concentration profile and we do not know whether the ^{18}O between the outer layer and the alloy–oxide interface represents a diffusion profile and hence the formation of new oxide at the alloy–oxide interface, or whether it represents the formation of new oxide within the original oxide layer. Buckling of the scale would indicate the latter, but the absence of buckling (as in this case) does not necessarily indicate the reverse, for if the scale consisted of polygonal grains, and if new oxide were formed

at grain-boundaries parallel to the oxide–metal interface, buckling of the oxide would not occur. The presence of whiskers on the inner surface of the oxide suggests that at least some new oxide was formed there. Gaseous transport of oxygen is unlikely to have taken place, because in that case we would have expected to observe a build-up of ^{18}O at the alloy–oxide interface, and we did not do so. Thus the results for these two specimens do not show evidence of the scale-cracking that has been suggested as an explanation of the 'linear' part of the oxidation kinetics for this alloy.

6. Conclusions

^{18}O tracer measurements have shown that the oxide scale that formed on a 20% (by mass) Cr, 25% (by mass) Ni, Nb-stabilized steel in CO_2 at 1123 K grew primarily by cation diffusion but that some oxygen diffusion also occurred. The scales have been shown to consist of an outer layer of spinel, inside that a layer of Cr_2O_3 and then a silicon-rich layer at the oxide–metal interface.

We are grateful to the Science Research Council for financial support for one of us (P.S.) and for a research grant which assisted the work, and to the Berkeley Nuclear Laboratories of the Central Electricity Generating Board for financial support and the provision of material.

References

Antill, J. E., Campbell, C. S., Goodison, D., Jepson, W. B. & Stevens, G. C. 1964 *Proc. 3rd Geneva Conf. Peaceful Uses of Atomic Energy*, vol. 9, pp. 523–528.
Antill, J. E. & Warburton, J. B. 1967 *Corros. Sci.* **7**, 645–649.
Calvert, J. M., Derry, D. J. & Lees, D. G. 1974 *J. Phys. D.* **7**, 940–953.
Evans, H. E., Hilton, D. A. & Holm, R. A. 1976 *Oxidat. Metals* **10**, 149–161.
Fern, F. H. & Antill, J. E. 1970 *Corros. Sci.* **10**, 649–655.
Francis, J. M. 1966 *J. Iron Steel Inst.* **204**, 910–913.
Francis, J. M., Curtis, M. T. & Hilton, D. A. 1971 *J. nucl. Mater.* **41**, 203–217.
Francis, J. M., Lee, C. J. & Buddery, J. H. 1968 *J. Iron Steel Inst.* **206**, 921–924.
Francis, J. M. & Whitlow, W. H. 1965 *J. Iron Steel Inst.* **203**, 468–473.
Hales, R., Smith, A. F. & Killeen, J. C. 1974 In *Corrosion of Steels in* CO_2 (ed. D. R. Holmes, R. B. Hill & C. M Wyatt), pp. 312–319. British Nuclear Energy Society.
Neild, D. J., Wise, P. J. & Barnes, D. G. 1972 *J. Phys. D.* **5**, 2292–2299.
Skeldon, P., Calvert, J. M. & Lees, D. G. 1980*a* *Phil. Trans. R. Soc. Lond.* A **296**, 557–565.
Skeldon, P., Calvert, J. M. & Lees, D. G. 1980*b* *Phil. Trans. R. Soc. Lond.* A **296**, 567–580.
Tyzack, C., Cowen, H. C., Farrow, M., Longton, P. B. & Whitlow, W. H. 1974 In *Corrosion of steels in* CO_2 (ed. D. R. Holmes, R. B. Hill & L. M. Wyatt), pp. 359–368. British Nuclear Energy Society.

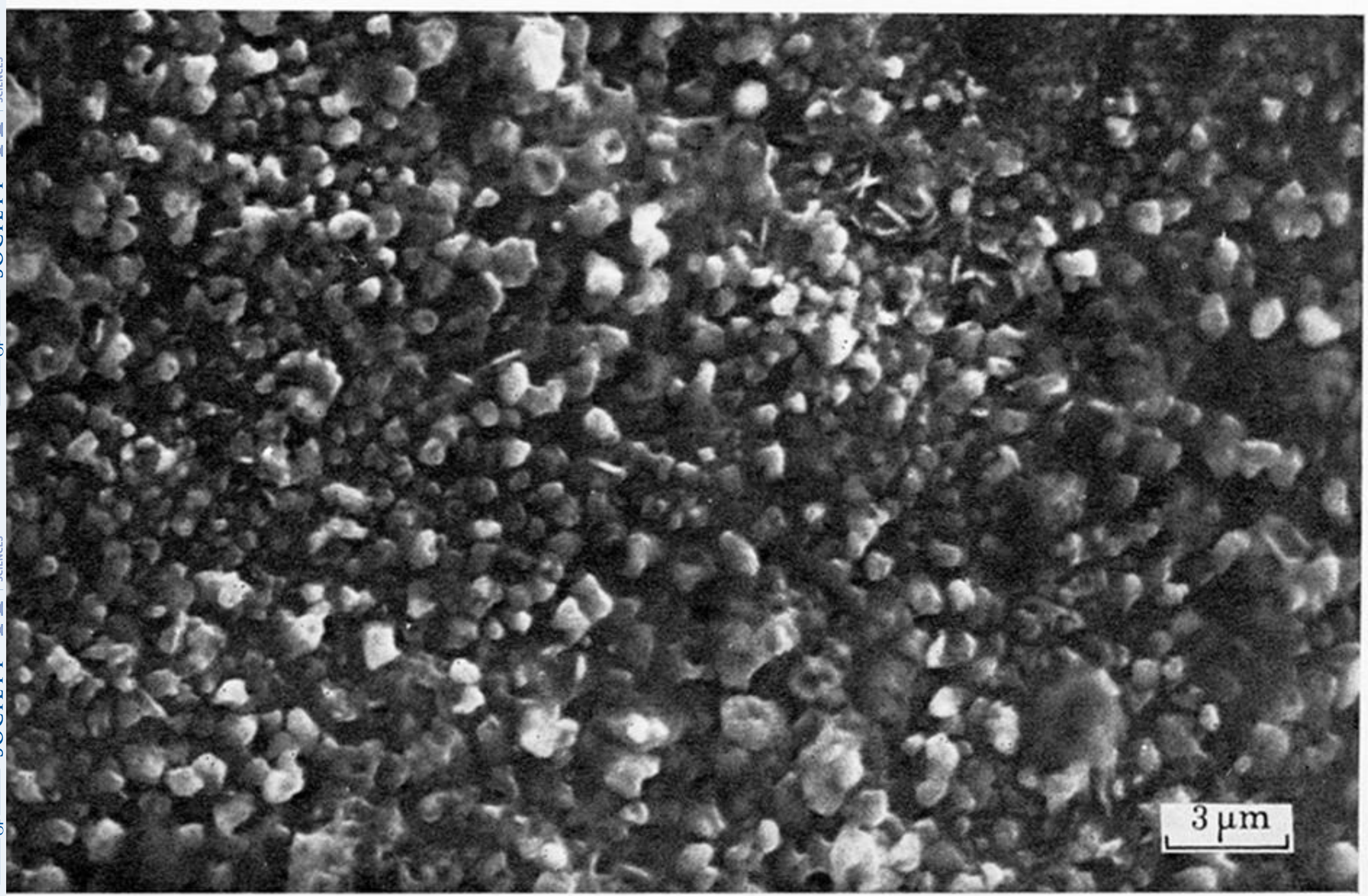

FIGURE 3. The surface of the scale on sample 1. Electron accelerating energy = 30 keV.

PHILOSOPHICAL TRANSACTIONS OF THE ROYAL SOCIETY A MATHEMATICAL, PHYSICAL & ENGINEERING SCIENCES

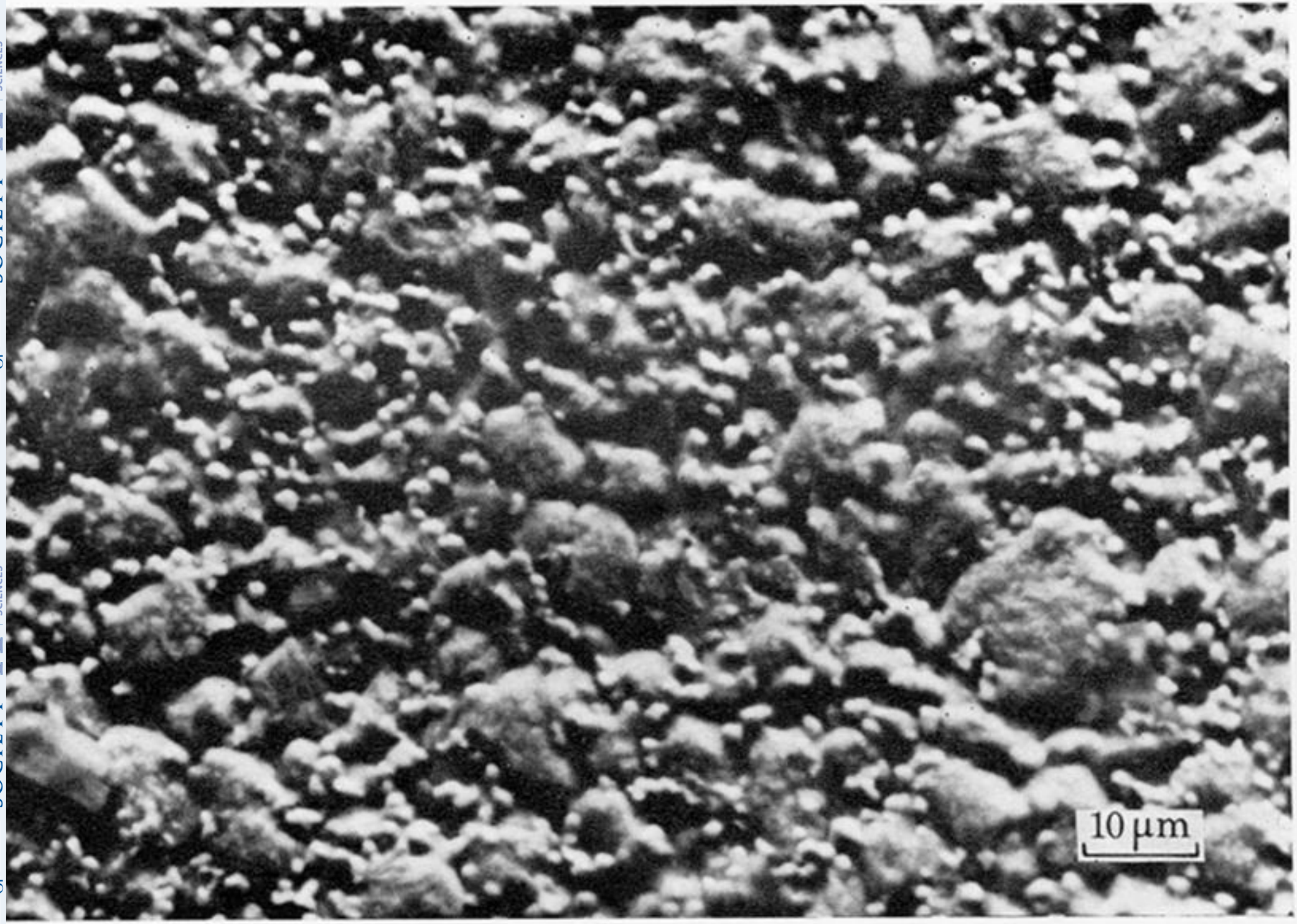

IGURE 5. The surface of sample 2, after oxidation and spallation of the scale. Electron acceleration energy = 30 keV.

PHILOSOPHICAL TRANSACTIONS OF THE ROYAL SOCIETY A MATHEMATICAL, PHYSICAL & ENGINEERING SCIENCES

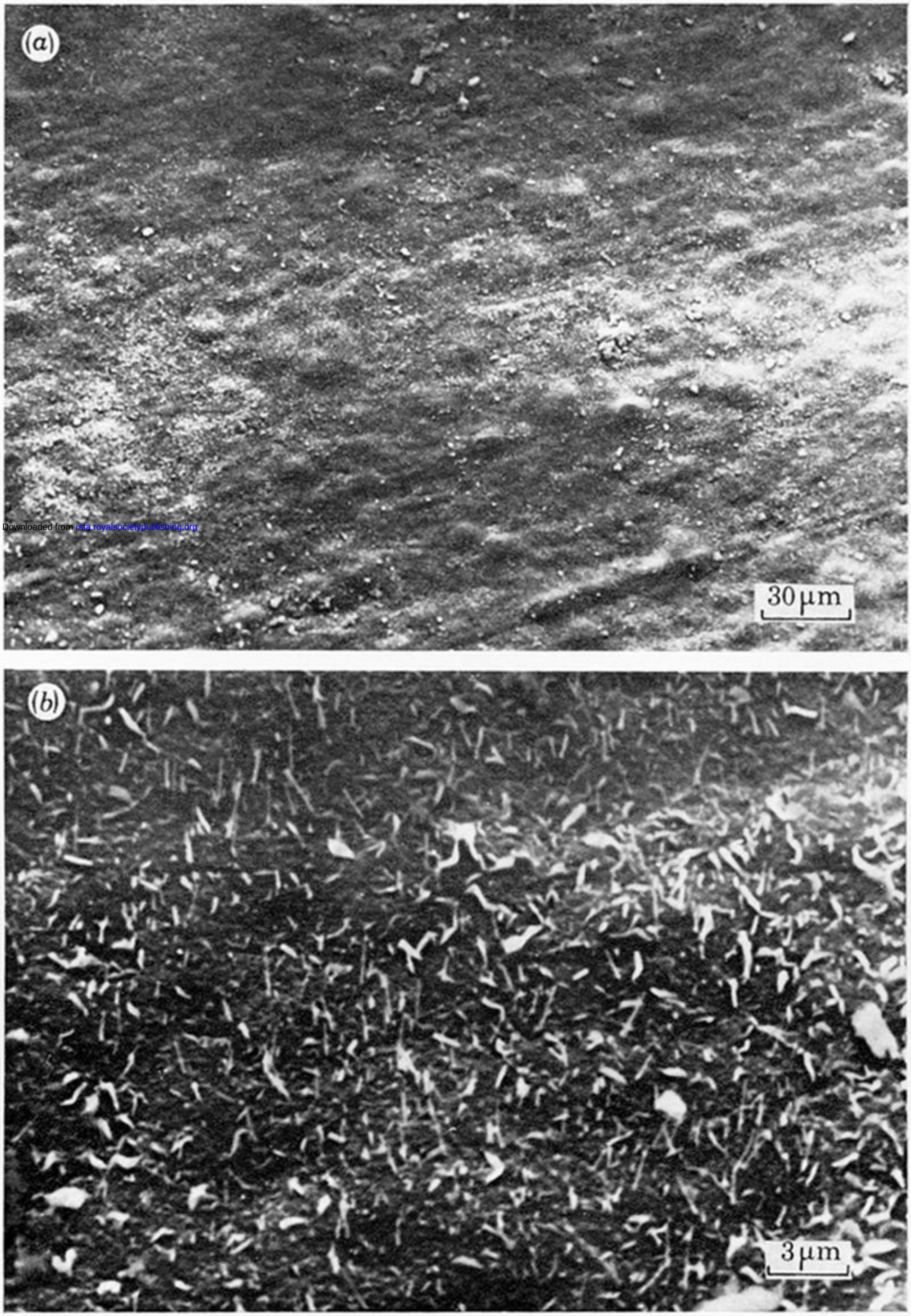

FIGURE 4. The underside of the scale formed on sample 2. Electron acceleration energy = 30 keV.